Arch. Metall. Mater. **70** (2025), 1, 477-488

DOI: https://doi.org/10.24425/amm.2025.152568

K. JANUS[1*], W. MAZIARZ[1], G. KORPALA[2], R. CHULIST[1], A. JARZĘBSKA[1], P. BALA[3], R. DZIURKA[3], U. PRAHL[2], L. ROGAL[1]

INFLUENCE OF MICROSTRUCTURE ON THE MECHANICAL PROPERTIES AND WORK-HARDENING BEHAVIOR OF HIGH-CARBON NANOSTRUCTURED BAINITIC STEEL

The microstructure-properties relationship of the low-alloy, high-carbon nanostructured bainitic steel obtained by heat treatment, including austenitization and cooling followed by isothermal nanobainitic transformation at 280°C for 72 h, was investigated. Detailed characterization of the obtained microstructure was performed using light optical, scanning, and transmission electron microscopy. These analyses reveals that the microstructure of tested nanobainitic steel consists of bainitic ferrite lath with an average size of 84 ± 21 nm and retained austenite with two different morphologies: (i) thin films with an average size of 64 ± 19 nm and (ii) blocks with a size of a few micrometers. The carbon concentrations in the film-type retained austenite and blocks of retained austenite were determined through X-ray synchrotron radiation diffraction analysis. The concentrations are 1.81 ± 0.09 wt.% and 1.39 ± 0.06 wt.%, respectively. The total amount of retained austenite in the microstructure is 48.0 ± 1.8 vol.%, and the dominant crystallographic orientation relationships between the microstructure constituents were determined to be Nishiyama-Wassermann. The minor K-S relationship was also recognized from the SEM/EBSD results. Tensile strength of the nanostructured steel was tested, and yield strength was found to be high. At an elongation of 7.2%, the tensile strength reached a significant level, while the average hardness was 490 ± 7 HV.

Keywords: Nanostructured bainitic steel; Microstructure; Mechanical properties; Austenite stability; TRIP effect

1. Introduction

Nanostructured bainitic steel continues to be a focus of scientific interest due to its high mechanical properties and relatively simple isothermal heat treatment resulting in a unique microstructure. This microstructure consists of bainitic ferrite laths supersaturated with carbon (α_b) and retained austenite (γ_R) in the form of thin films or blocks [1]. The size of these microstructural constituents are typically less than 100 nm to achieve high strength in the elastic deformation range due to grain refinement strengthening. In addition, the mechanical properties are improved by the high dislocation density and solid solution strengthening of α_b. Moreover, the transformation-induced plasticity (TRIP) of retained austenite and the appearance of twins in the film-type austenite are recognized as strain hardening mechanisms that enhance the ductility of this type of steel [2,3]. It should be noted that due to the addition of about 1 wt.% Si and 1 wt.% Al to the chemical composition of nanobainitic steel, as well as the trapping of carbon at accommodation twins and dislocations (Cottrell atmospheres), the obtained microstructure does not exhibit cementite precipitation, both within the bainitic ferrite laths and at the ferrite/austenite interfacial boundaries [4-6]. In addition, Beladi et al. [7] found that the crystallographic orientation relationship between bainitic ferrite and retained austenite of high-carbon nanostructured bainitic steel depends on the phase transformation temperature and changes gradually from Nishiyama-Wassermann (N-W) at 350°C to Kurdjumov-Sachs (K-S) at 200°C.

The nanomaterial can be obtained in all volumes of the manufactured specimens using phase transformation theory. This is possible if a bainitic transformation is carried out at a very low temperature, between 125-350°C, but above the martensitic starting temperature ($M_s^{\alpha'}$) and below the bainitic start temperature ($B_s^{\alpha_b}$) [8,9]. Allows to obtain as the temperature of nanobainitic transformation decreases, its total time increases (even up to 9 days at 200°C [10]), and the average size of bainitic ferrite plates and the amount of retained austenite blocks decrease. The nanobainitic microstructure obtained in this case is not thermo-

[1] INSTITUTE OF METALLURGY AND MATERIALS SCIENCE, POLISH ACADEMY OF SCIENCES, 25 REYMONTA STR., 30 059, KRAKOW, POLAND
[2] INSTITUT FÜR METALLFORMUNG, TU BERGAKADEMIE FREIBERG, BERNHARD-VON-COTTA-STRASSE 4,09596 FREIBERG, GERMANY
[3] AGH UNIVERSITY OF KRAKOW, FACULTY OF METALS ENGINEERING AND INDUSTRIAL COMPUTER SCIENCE, AL. A. MICKIEWICZA 30, 30-059 KRAKOW, POLAND

* Corresponding author: k.janus@imim.pl

dynamically stable because, during isothermal transformation, the carbon concentration in retained austenite is determined by the T_0' curve of the phase diagram. These factors are essential from a practical point of view because they directly determine the thermal and mechanical stability of austenite and influence the mechanical properties of nanostructured bainitic steels [8,11]. Avishan et al. [12] studied the structure-property relationships of two different chemical compositions of high-carbon nanobainitic steels focusing on the stability of retained austenite. The heat treatment carried out at 200°C for 3 days allows obtaining steels with similar ultimate tensile strength (~2.1 GPa) but different elongation. This difference of ~3.5% was attributed to the addition of Ni to the chemical composition, which affects chemical free energy change ($\Delta G^{\gamma\alpha'}$) for the transformation from austenite to martensite. This, in turn, influences the mechanical stability of retained austenite and the TRIP effect during deformation. In the other article, Avishan et al. [13] controlled the stability of retained austenite in the same high-carbon nanobainitic steels by adjusting heat treatment parameters, such as time and temperature. Both studies [12,13] confirm the significant impact of retained austenite stability on the obtained mechanical properties.

In another study [14], the authors applied isothermal heat treatment within a temperature range of 220-260°C for 24-4 h, respectively. The achieved tensile strength and elongation ranging from 2375 to 2080 MPa and 6.7 to 7.8%, respectively. These results indicated that lower transformation temperatures reduced the average size of the bainitic ferrite laths and increased their dislocation density, thereby increasing strength. At the same time, increasing the bainitic transformation temperature improved the mechanical stability of the retained austenite by altering its morphology and chemical composition.

The objective of this study was to investigate the influence of the microstructure of nanostructured bainitic steel on its mechanical properties and work-hardening behavior after isothermal heat treatment. The tested steel was subjected to low-temperature heat treatments, specifically isothermal holding at 280°C for 72 hours, to identify the correlation between microstructure and properties. Furthermore, the work-hardening exponent was used to analyze the work-hardening behavior during deformation, providing a more complete understanding of the mechanical stability of retained austenite. The factors influencing the mechanical properties of high-carbon nanostructured bainitic steel were identified and discussed.

2. Materials and experimental procedure

The chemical composition of the tested nanostructured bainitic steel was designed using the MUCG83 [15] and JMatPro software [16], thermodynamic models developed according to the phase transformation theory proposed by Bhadeshia and co-workers at the University of Cambridge. The resulting chemical composition of the low-alloy high-carbon steel was Fe-0.78C-1.67Si-2.45Mn-1.35Cr-0.21Mo-1.30Al (all in wt.%). This steel was subjected to a one-step austempering treatment, consisting of austenitization at 950°C for 30 minutes and isothermal treatment at 280°C for 72 hours. After austenitization, the steel was rapidly cooled at a rate of 10°C/s to prevent diffusion transformation. Prior to the austenitizing treatment, the tested steel was homogenized at 1250°C for 30 minutes and then hot-rolled at temperatures ranging from 1100°C to 850°C to achieve a 96% reduction in diameter. The homogenization and hot rolling process, crucial steps in our research, were performed to homogenize the dendritic segregation present in the cast steel, even after high-temperature annealing and the bainitic reaction, as demonstrated in our recent work [17] and noted by other authors [18,19]. The schematic of the austempering treatment applied is shown in Fig. 1.

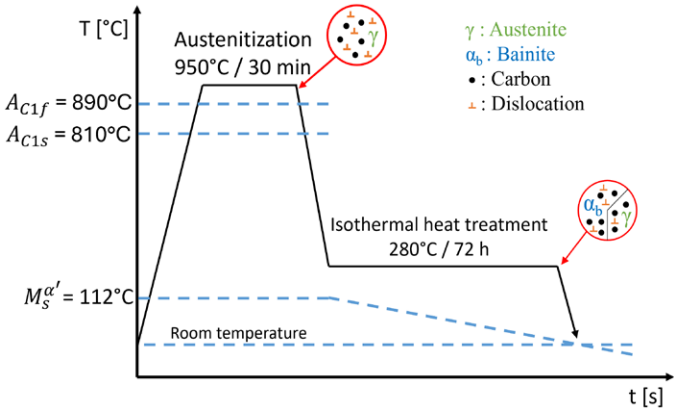

Fig. 1. Schematic illustration of the heat treatment applied to obtain the nanostructured bainitic steel

High-resolution dilatometric techniques utilizing the BAHR 805A dilatometer were used to design the one-step austempering treatment. To study the critical temperatures, such as A_{C_1}, A_{C_3} and $M_s^{\alpha'}$, and the kinetics of bainitic transformation in the tested steel, machined cylindrical specimens with a diameter of 4 mm and a length of 10 mm were used. Two types of dilatometric tests were carried out. First, the temperature range within which austenitization occurs and the martensitic start temperature, $M_s^{\alpha'}$ were determined during the thermal cycle experiment by drawing a tangent to the cooling curve. Secondly, the end of bainitic transformation (t_B) was determined from the kinetics of bainitic transformation at 280°C for 72 hours. In addition, the bainite start temperature $B_s^{\alpha_b}$ was calculated according to the literature equation [20]. During all tests, the temperature was controlled by a K-type thermocouple welded to the central part of the sample surface, with helium used as the control gas.

For qualitative and quantitative analysis of crystal structure, the high-energy X-ray synchrotron measurements were carried out using the beamline P07B (87.1 keV, λ = 0.0142342 nm) were caried out at DESY in Hamburg, Germany. The lattice parameters of the bainitic ferrite and retained austenite (a_{γ_R}), as well as their volume fraction were determined using HighScore Plus Software and the Rietveld refinement method. Based on

these results, the carbon concentration of retained austenite (C_γ) and bainitic ferrite (C_{α_b}) was calculated using Eq. (1) [21] and Eq. (2) [22], respectively:

$$C_\gamma \approx \frac{a_{\gamma_R} - 3.5780}{0.033} \tag{1}$$

$$\frac{a}{c} = 1 + 0.045 C_{\alpha_b} \tag{2}$$

where a and c are the lattice parameter of bainitic ferrite.

Additionally, the dislocation density of identified phases was calculated according to Eq. (3) [23]:

$$\rho = \frac{2\sqrt{3}\varepsilon^{21/2}}{Db} \tag{3}$$

where $\varepsilon^{21/2}$ is the lattice microstrain (derived from the measured broadening and 2θ position of peaks determined using the Williamson-Hall plot), b is a Burgers vector (for body-centered cubic (BCC) metals, b along <111> is $\frac{\sqrt{2}}{2}a_\alpha$, for face-centered cubic (FCC) metals, b along <110> is $\frac{\sqrt{3}}{3}a_\gamma$) in nm and D is a crystallite size for austenite and ferrite also determined from the Williamson-Hall plot.

To characterize the microstructure of the tested steel, a KEYENCE light optical microscope (LOM) and an FEI SEM XL30 scanning electron microscope (SEM/BSE) were used. Prior to observation, the steel specimens were ground using abrasive paper and then polished with 0.25 µm diamond polishing paste. The specimens were etched with a 4% Nital solution to reveal the microstructure after austempering treatment. Electron backscatter diffraction (EBSD) measurements were performed using the FEI Quanta 3D 200i FEG-SEM microscope. Mechanical grinding and final polishing with a colloidal silica slurry were performed to prepare the specimens for EBSD examination. The study was conducted using acceleration voltage of 20 kV, a tilt angle of 70°, and a step size of 0.1 µm. These parameters were used to investigate the orientation relationships between the microstructural constituents. Detailed observations of the microstructure were made using a transmission electron microscope (TEM) in bright field mode (TEM/BF), along with selected area diffraction (SAD) patterns, using a Tecnai G2 F20 transmission electron microscope. Thin films for observation were prepared by electropolishing with a Struers Tenupol-5 jet polisher, using an electrolyte composed of 20 vol% $HClO_4$ and 80 vol% CH_3OH at sub-zero temperatures. Following the literature [24] and using TEM analysis, the average thickness of the bainitic ferrite laths ($\bar{L}$) was measured by the relationship $\bar{L} = \pi t/2$, where t is the lath thickness. Mechanical properties were determined by Vickers hardness test under a load of 5 kg for 15 seconds on a Zwick/ZHU 250 testing machine and uniaxial tensile tests on a Bähr Thermoanalyse MDS 830 testing machine.

3. Results

3.1. Design the isothermal heat treatment of the tested steel

Fig. 2 shows the relative change in length (RCL) of the dilatometric sample as a function of temperature. The thermal cycle consisted of heating at 5°C/s to 950°C, holding for 5 minutes, and cooling at 10°C/s to room temperature. These steps allowed the determination of transformation temperatures such as $A_{c_{1s}}$, $A_{c_{3f}}$, and $M_s^{\alpha'}$ as 810°C, 890°C and 112°C, respectively. The applied cooling rate was sufficient to prevent diffusion transformation, and only martensitic transformation was detected. Furthermore, using the equation given in ref. [20], the $B_s^{\alpha_b}$ was calculated to be 316°C. Based on these results, the nanobainitic transformation window (the difference between $B_s^{\alpha_b}$ and $M_s^{\alpha'}$) was found to be 188°C. According to the nanobainitic theory [8], the isothermal transformation at 280°C was chosen, which allows for the formation of nanobainitic ferrite laths less than 100 nm and high dislocation density. The relative change in length (RCL) curve as a function of isothermal holding time, obtained from dilatometric tests, is shown in Fig. 3. This curve includes an incubation period where no transformation occurs, followed by a transformation period during which nucleation and growth of bainitic ferrite and carbon enrichment of retained austenite occur. Furthermore, in this case, the function $RCL = f(\log(time))$ reached a plateau after 72 hours of transformation, indicating that no further transformation of retained austenite to bainitic ferrite would occur. In addition, the change in RCL as a function of temperature shown in Fig. 3b confirms that the bainitic transformation time of 72 hours is sufficient to obtain a nanobainitic microstructure free from martensite precipitation, since the $M_s^{\alpha'}$ of the tested steel after isothermal holding is below 25°C. This suggests that during the bainitic transformation, carbon was redistributed and partitioned among the microstructural constituents produced, stabilizing the retained austenite at room temperature [25]. Therefore, to determine the bainitic transforma-

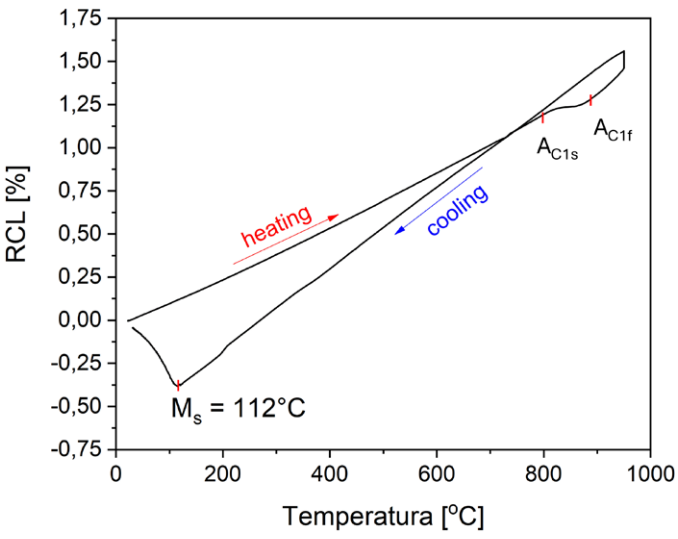

Fig. 2. The thermal cycle used to establish transformation temperatures

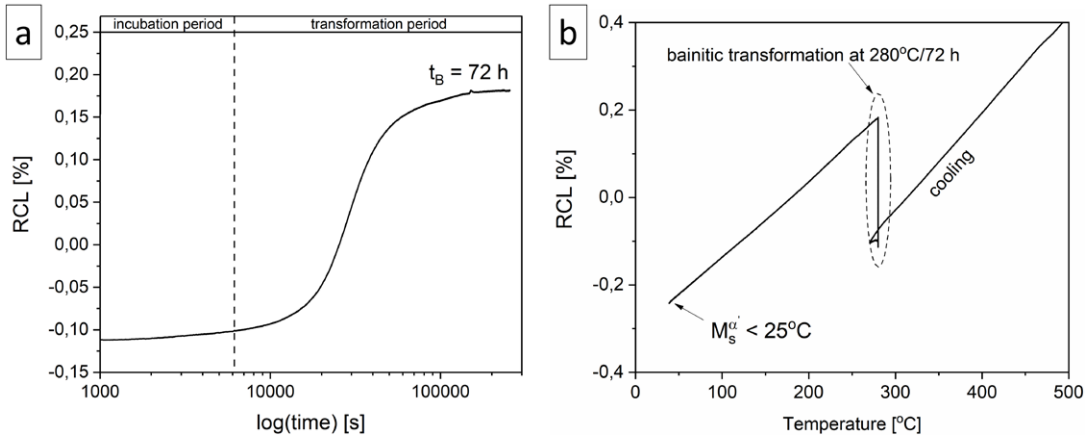

Fig. 3. The RCL as a function of (a) isothermal holding time and (b) temperature of the applied isothermal heat treatment

tion conditions, the heat treatment consisting of austenitization at 950°C for 30 minutes, rapid cooling at 10°C/s, isothermal holding at 280°C for 72 hours, and then quenching in water was carried out. Austenitization time was extended from 5 to 30 minutes because semi-industrial samples were used in the final one-step austempering treatment.

3.2. Microstructure analysis

Fig. 4 shows the high-energy synchrotron radiation diffraction pattern of the nanostructured bainitic steel obtained during the one-step austempering treatment. Two phases have been identified in the presented diffraction pattern. The face-centered cubic (FCC) and body-centered tetragonal (BCT) phases correspond to retained austenite (γ_R) and bainitic ferrite (α_b) with lattice parameters equal to 3.6257 Å (a_{γ_R}) and 2.8737 Å (a_{α_b}) and 2.8530 Å (c_{α_b}), respectively. The change in the crystal structure of bainitic ferrite from cubic to tetragonal in the nanobainitic steels is associated with an increase in the solid solubility of carbon, as demonstrated in previous research by *C.* Garcia-Mateo et al. [26]. In this work, the carbon concentration of bainitic ferrite was determined to be 0.17 ± 0.01 wt.% using Eq. (2), confirming the supersaturation of bainitic ferrite with carbon in the obtained nanobainitic steel. The volume fraction of retained austenite in the microstructure was estimated to be 48.0 ± 1.8 vol.%. The exceptionally high dislocation density in the bainitic ferrite laths was determined to be 5.80×10^{15} m^{-2}. It can be observed that the (200) peak of austenite is asymmetric and broadened. Therefore, according to the literature [27], it can be separated using the Gaussian multi-peak fitting method. This method allows this peak to be split into two individual peaks corresponding to the film-type retained austenite (red curve) and the blocky retained austenite (blue curve), as shown in Fig. 4b. Thus, using Eq. (1), the film-type retained austenite $\left(\gamma_R^f\right)$ with the carbon concentration $\left(C_\gamma^f\right)$ of 1.81 wt.% and the blocky retained austenite $\left(\gamma_R^b\right)$ with the carbon concentration $\left(C_\gamma^b\right)$ of 1.39 wt.% correspond to the peak with the lower (marked by the red line in Fig. 4b) and higher (marked by the blue line in Fig. 4b) 2θ values, respectively.

The microstructure of the investigated steel is shown in Fig. 5. The micrograph in Fig. 5a indicates that the obtained microstructure consists of bainitic sheaves and visible blocky retained austenite $\left(\gamma_R^b\right)$ with a size of a few micrometers. Subsequently, during SEM/BSE observation, it can be obtained that inside the bainitic sheaves, which are separated by the blocky

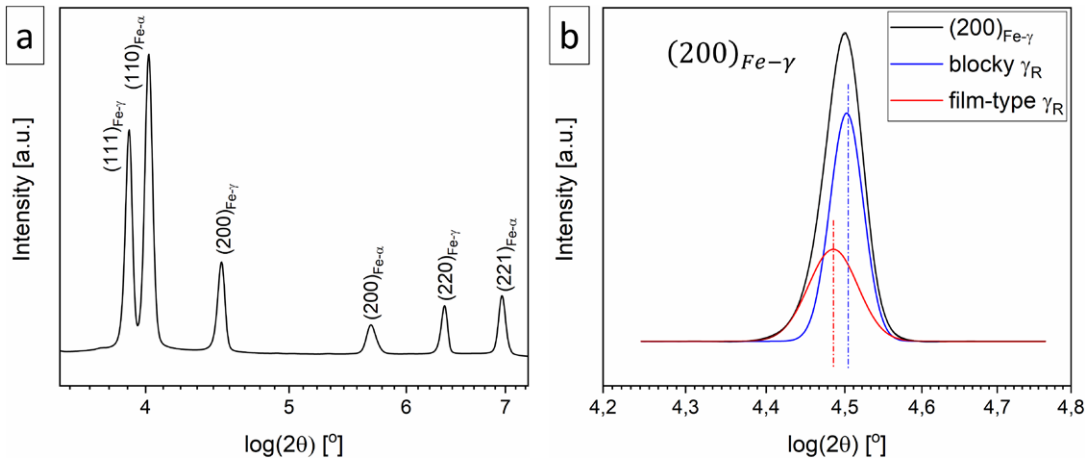

Fig. 4. (a) The high-energy synchrotron radiation diffraction pattern of tested nanostructured bainitic steel and (b) the zoom of a $(200)_{Fe-\gamma}$ with the division into film-type and blocky retained austenite

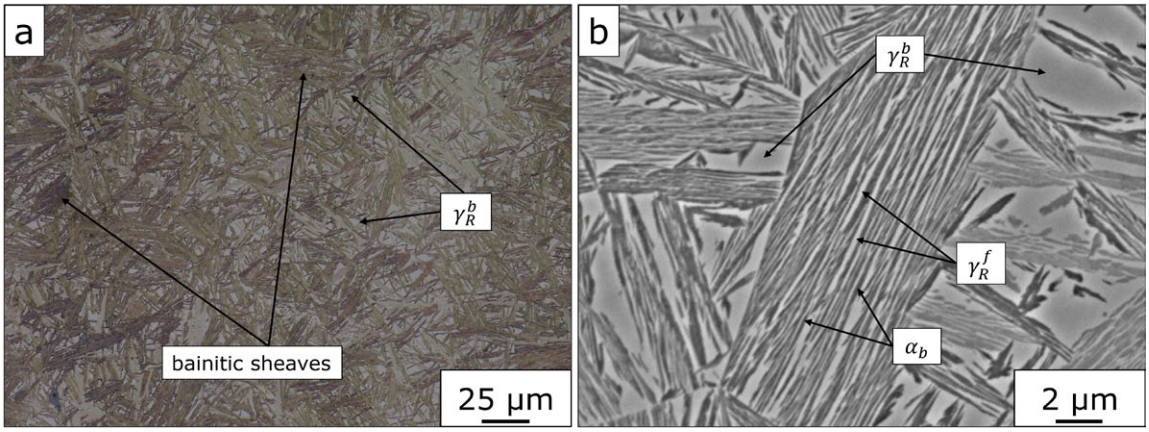

Fig. 5. (a) LOM and (b) SEM/BSE micrograph of semi-industrial samples subjected to one-step austempering treatment with isothermal holding at 280°C for 72 h

retained austenite from each other, the bainitic ferrite laths (α_b) and film-type of retained austenite (γ_R^f) were identified. Detailed observations of the microstructure were made by TEM examination, as shown in Fig. 6. These observations revealed that the microstructure consists of bainitic ferrite laths and retained austenite films with average sizes of 84 ± 21 nm and 64 ± 19 nm, respectively. The selected area diffraction pattern (Fig. 6b) from the area marked by the red circle in Fig. 6a allows the identification of α_b from strong reflections of $(110)_\alpha$ and $(10\bar{1})_\alpha$ planes with $[1\bar{1}1]_\alpha$ zone axis labeled in Fig. 6b. Similarly, the γ_R^f was determined from the weaker reflections of the $(020)_\gamma$ and $(111)_\gamma$ with $[\bar{1}0\bar{1}]_\gamma$ zone axis. In addition, based on the selected area diffraction pattern obtained from the marked area of the TEM/BF image (Fig. 6a), the orientation relationship between bainitic ferrite and retained austenite can be represented as the Kurdjumov-Sachs (K-S) relationship [21] and describes as follows: $(111)_\gamma \parallel (101)_\alpha$, $[\bar{1}10]_\gamma \parallel [1\bar{1}1]_\alpha$). Furthermore, based on TEM observation and high-energy synchrotron diffraction, no carbides were detected in the microstructure of the obtained nanostructured bainitic steel. This absence is attributed to the alloying of Si [4] and Al [5]. It has been shown that although these steels generally considered free of carbide precipitates, they are not completely free [28]. All the results obtained during the microstructural analysis of the nanobainitic steel using high-energy synchrotron radiation and TEM observations are summarized in TABLE 1.

Fig. 7a and Fig. 7b show the phase distribution map (PD), where the detected phases are marked in red for bainitic ferrite and green for retained austenite, respectively, along with the orientation map of these phases. The EBSD results were analyzed in the transverse direction to the deformation direction during the hot rolling process according to the stereographic triangle. From a single prior austenite grain marked by the black line in Fig. 7b, the directional distribution of specific orientation represented by pole figures (*PFs*) of {001} and {101} for bainitic ferrite and {001} and {111} for retained austenite were shown in Fig. 8. The crystallographic orientation relationships were presented in the form of the superposition of $\{001\}_{\alpha_b}$ and $\{001\}_{\gamma_R}$ as well as $\{101\}_{\alpha_b}$ and $\{111\}_{\gamma_R}$. The PFs of the recognized microstructure constituents exhibit characteristic features of the N-W orientation relationship, namely the four orientations of α_b in the middle of $\{001\}_{\alpha_b}$ pole figure, and the orientations at the $\{101\}_{\alpha_b}$, distributed in the shape of a triangle [29]. These features are marked by black circles in Fig. 8. To confirm the dominant orientation relationship between the bainitic ferrite and retained austenite, the misorientation distribution function (MDF) shown in Fig. 9 was examined using the entire EBSD dataset. This result indi-

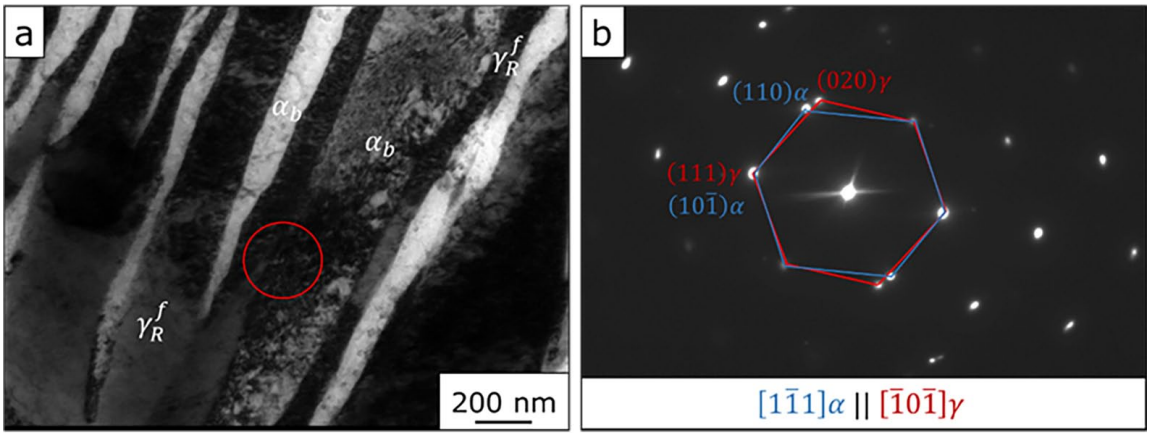

Fig. 6. (a) TEM/BF image and (b) corresponding SAD pattern from the area marked by the red circle of semi-industrial samples subjected to one-step austempering treatment with isothermal holding at 280°C for 72 h

TABLE 1

Characterization of microstructure constituents of obtained nanostructured bainitic steel

Bainitic ferrite laths (α_b)					
V_{α_b} [vol.%]	a_{α_b} [Å]	c_{α_b} [Å]	C_{α_b} [wt.%]	ρ_{α_b} [m^{-2}]	t_{α_b} [nm]
52.0 ± 1.2	2.8737 ± 0.0001	2.8530 ± 0.0001	0.17 ± 0.01	5.80×10^{15}	84 ± 21

Retained austenite (α_R)				
V_{γ_R} [vol.%]	a_{γ_R} [Å]	C_{γ_R} [wt.%]	ρ_{γ_R} [m^{-2}]	t_{γ_R} [nm]
48.0 ± 1.8	3.6257 ± 0.0001	1.42 ± 0.04	3.52×10^{14}	64 ± 19

Blocky retained austenite (α_R^b)		**Films of retained austenite (α_R^f)**	
$a^b_{\gamma_R}$ [Å]	$C^b_{\gamma_R}$ [wt.%]	$a^f_{\gamma_R}$ [Å]	$C^f_{\gamma_R}$ [wt.%]
3.6238 ± 0.0001	1.39 ± 0.06	3.6378 ± 0.0001	1.81 ± 0.09

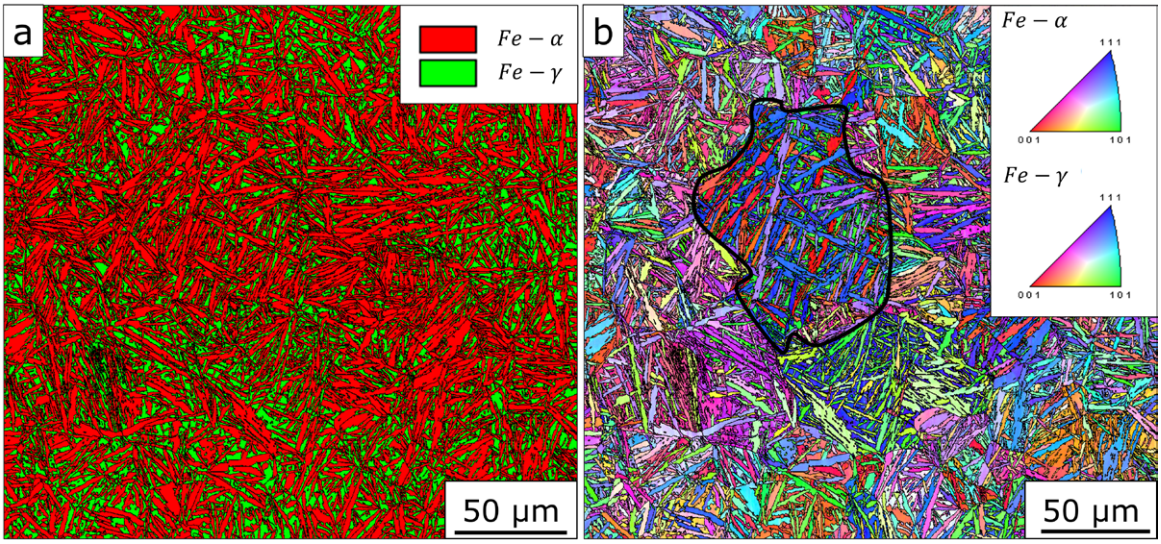

Fig. 7. (a) The phase color and (b) the PF maps of the manufactured nanostructured bainitic steel at 280°C/72 h. The PF map was colored according to the pole figures triangle shown in the right-up corner

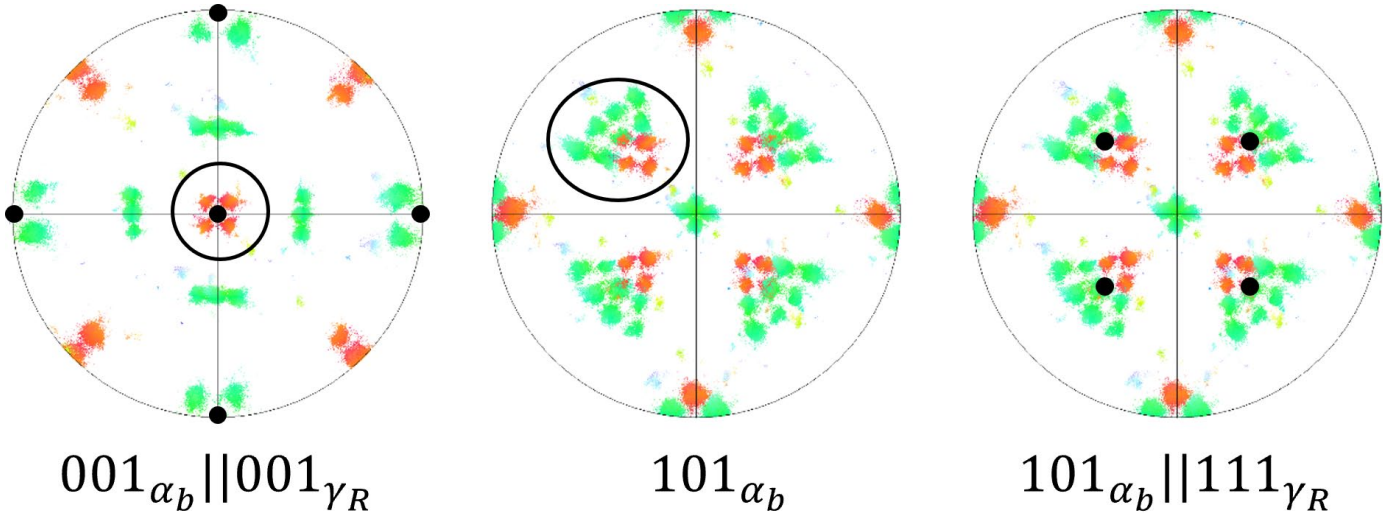

Fig. 8. Pole figures (PFs) from single prior austenite grain marked by black line in Fig. 7b represents by superpositions of $\{001\}_{\alpha_b}$ and $\{001\}_{\gamma_R}$ as well as $\{101\}_{\alpha_b}$ and $\{111\}_{\gamma_R}$ pole figures exhibiting the N-W relationship between bainitic ferrite and retained austenite. Austenite orientation is represented by black poles, while red and green correspond to different bainitic crystallographic variants

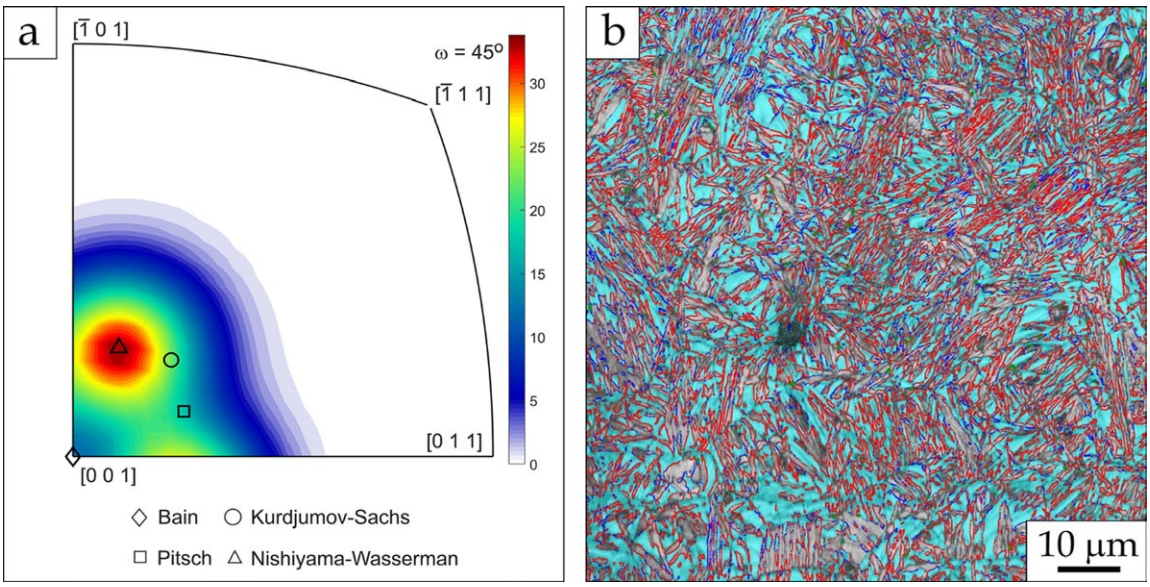

Fig. 9. (a) MDF for bainitic ferrite/retained austenite ORs with the key relation: Nishiyama-Wasserman (triangle), Kurdjumov-Sachs (circle), Pitsch (square), and Bain (diamond) and (b) PD map (ferrite-grey, austenite-blue) with the indicated N-W misorientation angles in red, K-S misorientation angles in navy blue, and Pitsch misorientation angle in green

cated that the dominant orientation relationship (OR) between α_b and γ_R is an N-W relationship, and the misorientation angle to 42.85° [30] was marked in red in Fig. 9b. Dworecka et al. in [31] also observed this relationship in high-carbon nanobainitic steel.

3.3. Mechanical properties

Fig. 10 shows the representative engineering stress-strain curve of the tested nanostructured bainitic steel. The mechanical properties determined were the ultimate tensile strength (UTS), yield strength (YS), and total elongation (A), which were 1386 ± 16 MPa, 989 ± 4 MPa, and 4.5 ± 0.4%, respectively. In addition, the Vickers hardness (HV5) of the manufactured nanostructured bainitic steel was 490 ± 7 HV5.

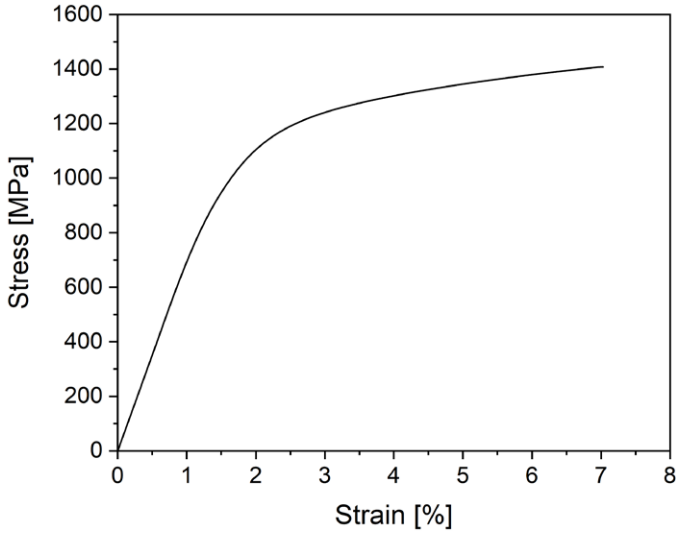

Fig. 10. The representative engineering stress-strain curve of the tested nanostructured bainitic steel

After uniaxial tensile deformation, structural analysis using high-energy synchrotron diffraction and transmission electron microscopy was performed near the fracture to explain the obtained mechanical properties. Fig. 11 shows the differences between the diffraction patterns of the tested nanobainitic steel before (black dashed line) and after (red line) tensile deformation. Based on these results, the amount of retained austenite was determined to be 43.1 ± 1.2 vol%, indicating that only 4.9 vol.% of the retained austenite transformed into martensite during deformation. This behavior indicates the high mechanical stability of the retained austenite.

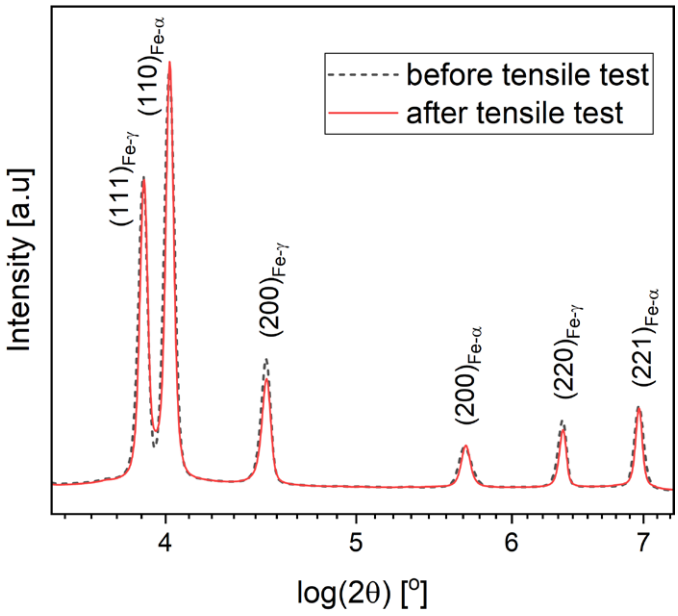

Fig. 11. The high-energy synchrotron diffraction patterns of tested steel before (black dashed line) and after (red line) tensile deformation

Detailed microstructural analysis of the tested nanostructured bainitic steel after tensile deformation reveals, in addition to the nanobainitic ferrite laths and retained austenite, the presence of twinned martensite (marked by white arrows in Fig. 12a). In Fig. 12, numerous parallel twinned martensite structures with an average thickness of a few nanometers and small inter-distance can be observed. The corresponding SAD pattern in Fig. 12b, obtained from the entire bright-field (TEM/BF) micrograph presented in Fig. 12a, clearly shows the {112} mirror symmetric diffraction pattern with the twinning plane (TP) parallel to it [32]. Martensite was most likely identified in the region of blocky retained austenite, as this form tends to undergo martensitic transformation during plastic deformation due to its lower carbon content compared to film-like retained austenite [33].

4. Discussion

Isothermal heat treatment at 280°C for 72 hours on steel with the chemical composition Fe-0.78C-1.67Si-2.45Mn-1.35Cr-0.21Mo-1.30Al (all in wt.%) has yielded significant findings. The evaluation of the microstructure-property relationship using optical microscopy, scanning and transmission electron microscopy, synchrotron radiation and uniaxial tensile testing has provided crucial insights. Nanobainitic steel requires a high carbon content of more than 0.6 wt.% to achieve the desired nanostructure in all sample volumes tested [34,35]. Alloying elements such as Co, Mo and Mn can partially substitute carbon to enhance the hardenability of the austenite [36,37]. However, these elements are used in minimal levels to reduce production costs, making a higher carbon concentration essential for stabilizing austenite. This high carbon concentration (0.78 wt.% in the presented results) presents challenges during the manufacturing, especially in controlling the isothermal transformation. The transformation temperature must be carefully controlled, as a low temperature can significantly increase the transformation time. At the same time, too high a temperature can lead to cementite precipitation in the nanobainite microstructure [25]. Another challenge is to determine the nanobainitic transformation time that achieves the desired microstructure of bainitic ferrite laths with an average size below 100 nm and thermally stable retained austenite. The carbon concentration in the retained austenite, an extremely important factor, plays a crucial role in its stability and determines the mechanical properties of the nanobainitic steel.

Isothermal heat treatment of high-carbon, low-alloy steels in the bainitic region above the $M_s^{\alpha'}$ temperature has been shown to produce distinct microstructures. The strength properties are primarily dependent on the thickness of the bainitic ferrite and its dislocation density [11, 38] In the case of the steel tested, an ultimate tensile strength of 1386 ± 16 MPa and a yield strength of 989 ± 4 MPa were achieved. This is attributed to the average thickness of the bainitic ferrite laths, which was measured to be 84 ± 21 nm. Additionally, the dislocation density in the bainitic ferrite was 5.80×10^{15} m^{-2}. According to theory, the strength enhancement due to the size and dislocation density of the bainitic ferrite is given by $\Delta\sigma_s = 115(\bar{L})^{-1}$ and $\Delta\sigma_d = 7.3410^{-6}(\rho_{\alpha_b})^{0.5}$, where $\bar{L} = 2t_{\alpha_b}$ in micrometers an $\Delta\sigma_{s,d}$ in MPa [39]. Applying these equations to the tested nanostructured bainitic steel, the $\Delta\sigma_s$ and $\Delta\sigma_d$ values of 685 MPa and 487 MPa, respectively, were obtained. Recent studies confirm that nanostructured bainitic ferrite exhibits a tetragonal crystal structure, as also observed in the tested steel. This structure allows more carbon to be incorporated into the solid solution than in the equilibrium state. The trapped carbon, located on dislocations near the austenite-ferrite interface and in Cottrell atmospheres, provides an additional obstacle to dislocation movement during deformation, thereby increasing the strength of the steel [39,40]. In the steel tested, the carbon concentration in bainitic ferrite was determined to be 0.17 ± 0.01 wt.%, confirming solid solution strengthening.

On the other hand, the amount of retained austenite primarily controls the ductility [33,41]. Despite the 48.0 ± 1.8 vol.% of retained austenite in the microstructure, the elongation was only 4.5 ± 0.4%. Sourmail et al. [41] suggested and confirmed that the mechanical stability of retained austenite is a more critical factor for achieving high ductility, which aligns with the present study. The mechanical stability of retained austenite depends mainly on its chemical composition, particularly its carbon concentration. These parameters are critical because they

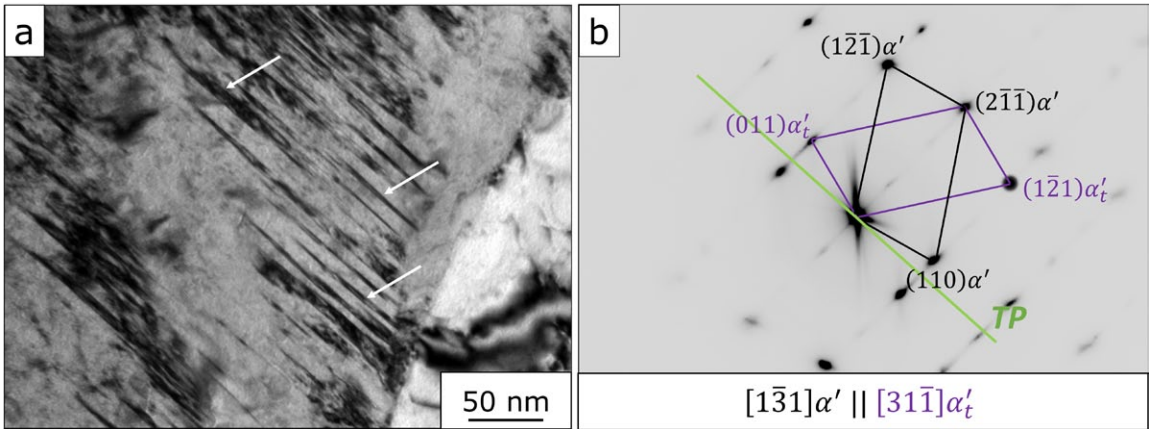

Fig. 12. (a) TEM/BF deformation microstructure and (b) corresponding SEAD pattern. TP – {112} Twinning Plane

significantly affect the $M_s^{\alpha'}$ temperature [33,43]. Two types of retained austenite morphologies were identified in the obtained microstructures: first, film-like retained austenite with a carbon concentration of 1.81 ± 0.09 wt.% and an average size of 64 ± 19 nm, and second, the blocky retained austenite with a carbon concentration of 1.39 ± 0.06 wt.% and a size of a few micrometres. Theoretical models suggest that the blocky retained austenite is thermodynamically more likely to transform into martensite during plastic deformation than the film-type due to its lower carbon content and consequently reduced mechanical stability [33]. At the same time, Avishan et al. [12] emphasized that the mechanical stability criterion is crucial for controlling the TRIP effect. Thus, the TRIP effect significantly influences the ductility of steel, and to evaluate this effect, the strain hardening exponent ($n = \partial \ln\sigma / \partial \ln\varepsilon$), where σ and ε refer to true stress and true strain, respectively) plays a key role and should be determined [42,44]. Therefore, the n vs. true strain relationship is shown in Fig. 13, where the retained austenite instability criterion is plotted. The red curve represents the strain-hardening exponent and reveals three main deformation stages, each critical for understanding the steel ductility process. Stage 1 can be attributed to densely distributed mobile dislocations in bainitic ferrite laths [45]. The rapid decrease between stages 1 and 2 is associated with the finer bainite microstructure, which hinders dislocation movement during plastic deformation [46]. At the beginning of stage 2, strain-induced martensite transformation (TRIP) occurs and the decrease in strain-hardening rate can be explained by the restriction of volume expansion due to martensite formation [47]. All residual austenite capable of transforming into martensite (with sufficient carbon content) undergoes the TRIP effect between stages 2 and 3, where the curve reaches a plateau [42]. To study the work-hardening mechanisms during the deformation process, three flow stress models can be utilized to reproduce the tensile curves: the Hallmon model (HM model), the Crussard-Jaoul (C-J) model, and the modified C-J model. The modified C-J model, chosen for this study, is particularly notable for its ability to adapt to changes in the work-hardening mechanism

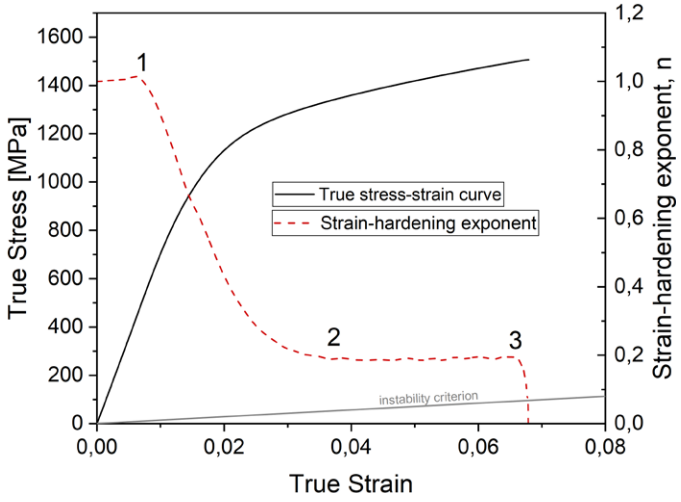

Fig. 13. The true stress-strain curve (black line) and strain-hardening exponent as a function of true strain (red dashed line)

at different stages of deformation, making it more suitable for analyzing the work-hardening behavior of multiphase steels [48]. Fig. 14 shows the plot of $\ln(d\sigma/d\varepsilon)$ versus $\ln\sigma$ or the tested nanostructured bainitic steel, which exhibits a decreasing slope of the curve. This analysis confirms the occurrence of three deformation stages during tensile deformation, corresponding to a high dislocation density within the bainitic ferrite laths, dislocations slip within the retained austenite, and martensitic transformation of the retained austenite blocks within the restricted strain range of 0.01 to 0.25 during the first and second stages, respectively. In the final (third) stage, all microstructural constituents are deformed, further demonstrating the adaptability of the modified C-J model, as evidenced by the steep slope of the curve in this stage.

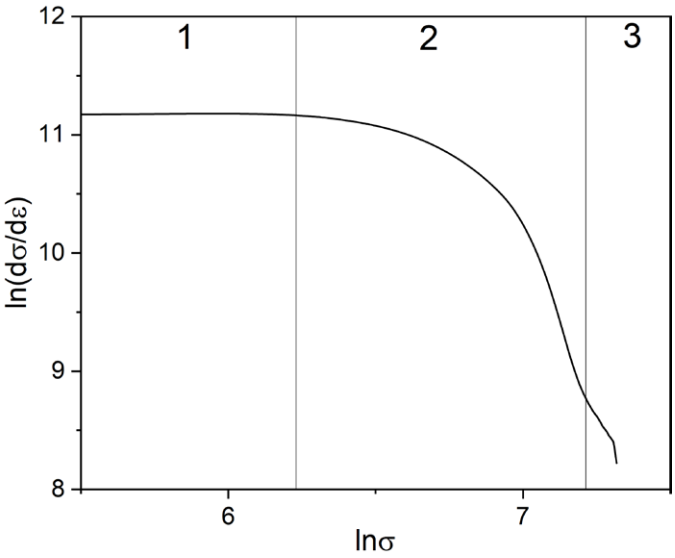

Fig. 14. Modified C-J analysis

It should be noted that the total amount of retained austenite after tensile test was 43.1 ± 1.2 vol.%. Compared to the initial conditions before tensile testing, only 4.9 vol.% of retained austenite was transformed into martensite during tensile deformation. C. Garcia-Mateo et al. [33] pointed out that large amounts of stable austenite at necking (instability criterion, $\varepsilon = n$) do not guarantee increased ductility if the austenite is too mechanically stable. A similar situation was observed in the tested steel. The film-like retained austenite, with an average carbon concentration of 1.81 ± 0.09 wt%, is too stable to transform into martensite during tensile deformation once the yield strength of the retained austenite is reached [49]. In contrast, the less stable, blocky retained austenite, with a lower carbon content of 1.39 ± 0.06 wt.%, is more susceptible to strain-induced plasticity effects. As documented in the literature [33,49], the carbon concentration in retained austenite depends on its morphology: film-like austenite typically contains higher carbon content, while blocky austenite has lower carbon content. As shown in Fig. 5, retained austenite blocks vary significantly in size, leading to inhomogeneous carbon distribution within a single block [50]. This variation in carbon content can cause parts of the blocks with lower carbon

content to deform, while regions with higher carbon content remain too mechanically stable. Therefore, the TRIP effect is observed in Fig. 12, but only within a limited deformation range. It can be concluded that the limiting carbon content required for the mechanical stabilization of retained austenite in the tested steel is approximately 1.39 wt.%. Tan et al. [51] suggest that the limiting carbon content needed to achieve an $M_s^{\alpha'}$ temperature below 25°C is 0.92 wt.%. Meanwhile, the mechanical stability of retained austenite suitable for TRIP transformation is ensured by a carbon content between 0.92 and 1.31 wt.%.

Fig. 12 and Fig. 13 illustrate that the TRIP effect occurred within a narrow strain range during the tensile tests on the steel. This is because the carbon content in the retained austenite blocks varied, resulting in only a small fraction of the austenite having sufficient mechanical stability to undergo the TRIP effect. The Stacking Fault Energy (SFE) of the investigated retained austenite, as calculated from the literature [52], is 21.36 mJ/m^2, which confirms that the TRIP effect should occur during deformation. In summary, the carbon content in retained austenite is influenced by both the temperature and time of the bainitic transformation, in accordance with the T_0 temperature theory [8,11]. As the temperature increases, the carbon content in retained austenite decreases, because the time required to complete the bainitic transformation shortens, thereby reducing its mechanical stability and enhancing the efficiency of martensitic transformation during deformation. This change improves the ductility of the tested steel, though it may lower its strength due to factors such as the increased average size of the bainitic ferrite laths. Additionally, it is essential to consider the mechanical stability of retained austenite in terms of its morphology (e.g., as films and blocks) and to focus on the carbon content variation within the blocky austenite. The variation in carbon content, related to the size of the blocks, significantly affects the achievement of high ductility in the steel under investigation.

Compared to other high-carbon nanobainitic steels produced through conventional heat treatment processes, the mechanical properties of the experimental steel are relatively lower. For example, at an isothermal holding temperature of 200°C, Avishan et al. [13] achieved UTS, YS, and elongation values of 2115 MPa, 1405 MPa, and 8%, respectively. Considering the inhomogeneous distribution of carbon content in blocky austenite, detailed TEM observations of the initial microstructure (before tensile testing), as shown in Fig. 15, revealed stacking faults in the retained austenite films. These were likely caused by the accumulation of shear stress in the microstructure during the bainitic transformation. Additionally, carbide precipitates were observed within the bainitic ferrite laths, which were not detected in the synchrotron radiation studies (Fig. 4 and Fig. 11) and are indicated by a red arrow in Fig. 15. These factors directly contributed to the reduction in elongation [7,53], as the TWIP effect induced by the bainitic transformation limited the activation of this strengthening mechanism during tensile testing. On the other hand, the carbide precipitations may have resulted from either too low an isothermal holding temperature [8] or an excessively long heat treatment time [54], leading to the self-tempering of the microstructure. Based on the literature [55], these precipitates are likely cementite or other n-carbides. These observed changes in microstructure, along with the variation in carbon content within blocky austenite, further influenced the mechanical properties, reducing the UTS and elongation of the experimental steel. The interplay of these factors underscores the complexity of our research.

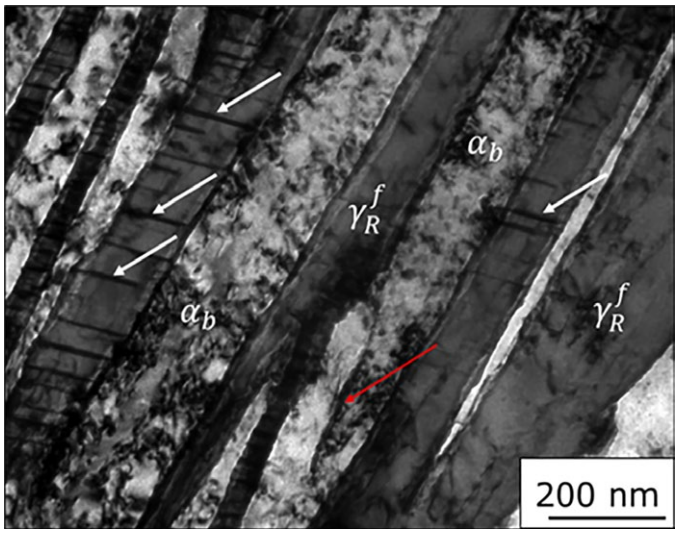

Fig. 15. TEM/BF image of semi-industrial samples subjected to a one-step austempering treatment with isothermal holding at 280°C for 72 hours. The white arrows indicate the stacking faults, while the red arrow points to a carbide

5. Consclusions

In this study, the relationship between microstructure and properties of high-carbon, low-alloy nanostructured bainitic steel was investigated. Based on the results, the following conclusions were formulated:

1. Developed conditions of heat treatment, which included austenitization at 950°C for 30 min followed by cooling to 280°C with isothermal holding for 72 hours, allow obtaining the nanostructured bainitic steel. The resulting microstructure consisted of bainitic ferrite laths and thin films of retained austenite with an average size of 84 ± 21 and 64 ± 19 nm, respectively. Simultaneously, the content of retained austenite (both blocky and film-type) in the obtained microstructure is 48.0 ± 1.8 vol.%. In addition, the Nishiyama-Wassermann crystallographic orientation relationship between the bainitic ferrite plates and retained austenite was identified based on the EBSD measurements. The dominant relationship had a misorientation angle of 42.85°.
2. The applied isothermal heat treatment produced retained austenite in the form of thin films with average carbon concentrations of 1.81 ± 0.09 wt.% and blocky retained austenite with an average carbon concentrations of 1.39 ± 0.06 wt.%. These carbon concentration directly influenced the mechanical stability of the retained austenite and

its potential for transformation into martensite. The TRIP effect, assessed via strain-hardening exponent analysis, was confirmed to occur during tensile deformation. However, it was observed within a limited strain range (0.01-0.25). The limited elongation of the nanostructured bainitic steel was attributed to the high mechanical stability of the blocky austenite, which resulted from carbon concentration fluctuations depending on the size and morphology of the austenite.

3. The strain-hardening exponent, together with the modified C-J model, revealed that the work-hardening of the tested steel during tensile deformation can be divided into three main stages: (i) the dense dislocation movement within the bainitic ferrite laths, (ii) the martensitic transformation of retained austenite blocks, and (iii) the deformation of all microstructural constituents.

The high strength of the nanostructured steel, with an ultimate tensile strength of 1386 ± 16 MPa and yield strength of 989 ± 4 MPa, was obtained due to a nanometric size of bainitic ferrite plates (84 ± 21 nm), their high dislocation density (5.80×10^{15} m^{-2}), and the increased solubility of carbon in bainitic ferrite solid solution (0.17 ± 0.01 wt.%). Meanwhile, compared to other high-carbon nanobainitic steels, the mechanical properties of the tested steel were relatively lower. This reduction in performance has been attributed to the inhomogeneous distribution of carbon within the blocky austenite, the twinning of retained austenite films, and the precipitation of carbides during isothermal heat treatment at 280°C for 72 h.

Acknowledgments

This research was supported by The National Research and Development Centre, Poland (Project No POIR.01.01.01-00-0418/19-00).

REFERENCES

[1] C. Garcia-Mateo, F.G. Caballero, T. Sourmail, M. Kuntz, J. Cornide, V. Smanio, R. Elvira, Materials Science and Engineering: A **549**, 185-192 (2012).

[2] L. Morales-Rivas, C. Garcia-Mateo, T. Sourmail, M. Kuntz, R. Rementeria, G. Caballero, Metals **6** (12), 302 (2016).

[3] K. Janus, L. Rogal, J. Dutkiewicz, R. Chulist, G. Korpala, U. Prahl, K. Konczak, P. Kochmanski, K. Nalepka, W. Maziarz, Archives of Civil and Mechanical Engineering **23**, 252 (2023).

[4] S. Lin, A. Borgenstam, A. Stark, P. Hedström, Materials Characterization **185**, 111774 (2022).

[5] L. Liu, B. He, M. Huang, Advanced Engineering Materials **20** (6), 17001083 (2018).

[6] F.G. Caballero, H.W. Yen, M.K. Miller, J.R. Yang, J. Cornide, C. Garcia-Mateo, Acta Materialia **59** (15), 3117-6123 (2011).

[7] H. Beladi, V. Tari, I.B. Timokhina, P. Cizek, G.S. Rohrer, A.D. Rollett, P.D. Hodgson, Acta Materialia **127**, 426-437 (2017).

[8] H.K.D.H. Bhadeshia. Bainite in Steels: Theory and Practice, 3rd Edition. Taylor & Francis Group, London (2015).

[9] F.G. Caballero, C. Garcia-Mateo, M.K. Miller, The Journal of The Minerals, Metals & Materials Society (TMS) **66** (5), 747-755 (2014).

[10] C. Garcia-Mateo, F.G. Caballero, H.K.D.H. Bhadeshia, SIJ International **43**, 1238-1243 (2003).

[11] H.K.D.H. Bhadeshia, Proc Roy Soc Lond A **466**, 3-18 (2010).

[12] B. Avishan, C. Garcia-Mateo, L. Morales-Rivas, S. Yazdani, F.G. Caballero, Journal of Materials Science **68**, 6121-6132 (2013).

[13] B. Avishan, S. Yazdani, F.G. Caballero, T.S. Wang, C. Garcia-Mateo, Materials Science and Technology **31** (12), 1508-1520 (2015).

[14] J. Yang, T.S. Wang, B. Zhang, F.C. Zhang, Materials & Design **35**, 170-174 (2012).

[15] https://www.phase-trans.msm.cam.ac.uk/map/steel/programs/mucg83.html, online: 21/08/2023

[16] https://www.sentesoftware.co.uk/jmatpro, online: 21/08/2023

[17] P. Garbień, A. Kokosza, W. Maj, Ł. Rogal, R. Chulist, K. Janus, A. Wójcik, Z. Żółkiewicz, W. Maziarz, Archives of Metallurgy and Materials **68** (4), 1667-1676 (2023).

[18] F.G. Caballero, J. Chao, J. Cornide, C. García-Mateo, M.J. Santofimia, C. Capdevila, Materials Science and Engineering: A **525**, 87-95 (2009).

[19] Y. Guo, Z. Li, C. Yao, K. Zhang, F. Lu, K. Feng, J. Huang, M. Wang, Y. Wu, Materials & Design **63**, 100-108 (2014).

[20] J. Trzaska, Archives of Metallurgy and Materials **60**, 1, 181-185 (2015).

[21] H. Beladi, Y. Adachi, I. Timokhina, P.D. Hodgson, Scripta Materialia **60** (6), 455-458 (2009).

[22] A. Królicka, F.G. Caballero, R. Kuziak, K. Radwański, L. Sozańska-Jędrasik, P. Stawarczyk, Journal of Materials Research and Technology **24**, 7004-7020 (2023).

[23] G. Dini, R. Ueji, A. Najafizadeh, S.M. Monir-Vaghefi, Materials Science and Engineering: A **527** (10-11), 2759-2763 (2010).

[24] C. Garcia-Mateo, J.A. Jimenez, B. Lopez-Ezquerra, R. Rementeria, L. Morales-Rivas, M. Kuntz, F.G. Caballero, Materials Characterization **122**, 83-89 (2016).

[25] M.A. Santajuana, A. Eres-Castellanos, V. Ruiz-Jimenez, S. Allain, G. Geandier, F.G. Caballero, C. Garcia-Mateo, Metals **9** (9), 925 (2019).

[26] C. Garcia-Mateo, J.A. Jiménez, H.W. Yen, M.K. Miller, L. Morales-Rivas, M. Kuntz, S.P. Ringer, J.R. Yang , F.G. Caballero, Acta Materialia **91**, 162-173 (2015).

[27] X. Wang, C. Liu, Y. Qin, Y. Li, Z. Yang, X. Long, M. Wong, F. Zhang, Materials Science and Engineering: A **832**, 142357 (2022).

[28] C. Hofer, F. Winkelhofer, J. Krammerbauer, H. Clemens, S. Primig, Materials Today: Proceedings **2**, S925-S928 (2015).

[29] F. Barcelo, J.L. Bechade, B. Fournier, Phase transitions **83** (8), 601-614 (2010).

[30] K. Nalepka, B. Skoczeń, M. Ciepielowska, R. Schmidt, J. Tabin, E. Schmidt, W. Zwolińska-Fryj, R. Chulist, Materials **14** (1), 127 (2021).

[31] J. Dworecka, E. Jezierska, J. Rębiś, K. Rożniatowski, W. Świątnicki, Archives of Metallurgy and Materials **59** (4), 1633-1636 (2014).

[32] X.C. Xiong, B. Chen, M.X. Huang, J.F. Wang, L. Wang, Scripta Materialia **68** (5), 321-324 (2013).
[33] C. García-Mateo, F.G. Caballero, Materials Transactions **46** (8), 1839-1846 (2005).
[34] K. Wasiluk, K. Wasiak, E. Skołek,W. Świątnicki, Metal 1-7 (2014).
[35] M. Akram, H. Palkowski, M. Soliman, Steel Research International (2021).
[36] M.S. Węglowski, J. Marcisz, B. Garbarz, Biul. Inst. Spaw. 29-43 (2018).
[37] A. Królicka, A.M. Żak, F.G. Caballero, Materials & Design **211**, 110143 (2021).
[38] B. Avishan, S.M. Khoshkebari, S. Yazdani, Materials Chemistry and Physics **260**, 124160 (2021).
[39] C. Garcia-Mateo, F.G. Caballero, H.K.D.H. Bhadeshia, Materials Science Forum **500-501**, 495-502 (2005).
[40] H. Meng, Z. Hong, Y. Li and X. Jia, Z Yin, Metals **11** (12), 2007 (2021).
[41] T. Sourmail, C. Garcia-Mateo, F.G. Caballero, L. Morales-Rivas, R. Rementeria, M. Kuntz, Metals **7** (1), 31 (2017).
[42] X. Yu, H. Wu, Y. Gu, R. Yuan, Y. Zhang, Y. Feng, Journal of Iron and Steel Research International **29**, 647-654 (2022).
[43] B.C. De Cooman, Current Opinion in Solid State and Materials Science **8** (4-3), 285-303 (2004).
[44] T. Wang, L. Qian, K. Li, F. Zhang, J. Meng, Materials Science and Engineering: A **819**, 141498 (2021).
[45] A. Barbacki, Journal of Materials Processing Technology **53** (1-2), 57-63 (1995).
[46] A. Kumar, S.B. Singh, K.K. Ray, Materials Science and Engineering: A **474** (1-2), 270-282 (2008).
[47] S.M. Hasan, A. Mandal, S.B. Singh, D. Chakrabarti, Materials Science and Engineering: A **751**, 142-153 (2019).
[48] T. He, L. Wang, F. Hu, W. Zhou, Z. Zhang, K. Wu, Journal of Materials Research and Technology **22**, 2690-2703 (2023).
[49] X. Wang, C. Liu, Y. Qin, Y. Li, Z. Yang, X. Long, M. Wang, F. Zhang, Materials Science and Engineering A **832**, 142357 (2022).
[50] J. Zhao, B. Lv, F. Zhang, Z. Yang, L. Qian, C. Chen, X. Long, Materials Science and Engineering: A **742**, 179-189 (2019).
[51] X. Tan, D. Ponge, W. Lu, Y. Xu, H. He, J. Yan, D. Wu, D. Raabe, Acta Materialia **186**, 374-388 (2020).
[52] S. Curtze, V.T. Kuokkala, Acta Materialia **58** (15), 5129-5141 (2010).
[53] A. Kumar, A. Singh, Materialia **15**, 101034 (2021).
[54] M.A. Santajuana, A. Eres-Castellanos, V. Ruiz-Jimenez, S. Allain, G. Geandier, F.G. Caballero, C. Garcia-Mateo, Metals **9** (9), 925 (2019).
[55] S. Ghosh, K. Rakha, S. Reza, M. Somani, J. Kömi, Materials Today: Proceedings **62** (14), 7570-7573 (2022).